Optics Letters

Critical phenomenon in tapered dielectric structures

ADI HANUKA* AND LEVI SCHÄCHTER

Department of Electrical Engineering, Technion–Israel Institute of Technology, Haifa 32000, Israel
**Corresponding author: Adiha@tx.technion.ac.il*

Received 6 July 2017; revised 23 September 2017; accepted 27 September 2017; posted 28 September 2017 (Doc. ID 301666); published 26 October 2017

We demonstrate the existence of a critical behavior of a single electromagnetic mode propagating in a tapered dielectric structure. This behavior is described in terms of a critical phase velocity in the case of an adiabatic tapering. In the vicinity of this critical phase velocity, the tapered structure no longer confines the radiation and a significant fraction of the power escapes transversely.

OCIS codes: (230.0230) Optical devices; (350.5610) Radiation; (260.2030) Dispersion.

https://doi.org/10.1364/OL.42.004458

There is a growing demand for compact optical components that can be integrated on-chip, to increase portability and potentially reduce the cost and complexity of today's systems [1]. This is true for various fields, among them high-resolution spectrometry [2], sensing [3], communication [4], accelerators [5], high-power lasers [6,7], and high-energy applications.

Tunable dielectric quasi-periodic structures can be used as building blocks for such integrated optics. As low-loss periodic dielectrics, which control light propagation, Bragg waveguides [8] and photonic band-gap (PBG) fibers [9–12] are key elements for a variety of applications, for example, mode filtering 13,14]], tunable lasers [15], multi/demultiplexing [4], coupling [16,17], mode conversion [18], field concentration [19], and polarization dispersion compensation and manipulation [20].

Common to all quasi-periodic structures is a core (vacuum or dielectric) surrounded by a cladding structure that facilitates confinement—for example, multilayers in Bragg waveguides or a pattern of holes in PBG. In order to tune the structure, both the material and the tapering shape of either the core tunnel or the quasi-periodic structure should be considered.

Previous studies [21–25] have suggested several tapered configurations as shown in Figs. 1(a)–1(c). With regard to dielectric materials (core or clad), it was suggested (see the two top frames in Fig. 1) to define either a *linear* or *exponential* taper of the waveguide's width [23] using a traveling burner tapering method [24,25]. With regard to a hollow core fiber, it was suggested to define a linear taper of the core's width with wafer bonding by either a photo-resist spacing post [21] and epoxy "posts" [22], sacrificial etching techniques, or the buckling self-assembly process [26]. However, the restriction on the hollow core's dimensions is a serious impediment.

It was shown experimentally [27,28] that in a system with a linearly tapered vacuum core [Fig. 1(c)], radiation propagates transversally when operating *below cutoff*. However, operating with a single mode *far from cutoff* by retaining the vacuum core's width fixed, opens a wide range of applications. In spectroscopy, for example, optimal resolution is achieved when only the lowest-order mode is excited [27]. Similarly, in laser-driven particle accelerators, a single TM_{01} mode is co-propagating with the particle, and the former phase velocity should be synchronized to the velocity of the particle [29].

In this study, we introduce a novel tapering method whereby the radius of the vacuum core is kept *constant*, while the adiabatic tapering is determined by the *local* phase velocity. The latter depends on the longitudinal structure's coordinate (z-axis) [29]; however, this is beyond the scope of this study. As a result, there is a global change of all layers, and the thickness of each layer varies along the z-axis of the structure. This is different than the linear or exponential tapering of the core or clad, whereby the geometry of the layers is kept globally constant but they are either tilted or drawn.

With regard to confinement, we show a critical phenomenon in which a single propagating mode (wavelength λ), leaks out—not due to a finite number of layers [13]—but because it reaches a critical point where a longitudinal flow of electromagnetic power is transformed into a transverse propagation.

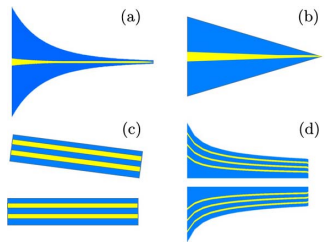

Fig. 1. Types of Bragg waveguide tapering profiles; (a) exponential or (b) linear taper for dielectric core fiber—which confines light although some transmission losses [24], (c) tilted wafer bonding, and (d) suggested configuration for hollow core fiber.

This mode is far from the cutoff, contrary to leaky mode [30] which is defined near cutoff [31]. Contrary to the linear tapering [27,28], whereby transverse propagation is a direct result of cutoff ($k_z^2 \le 0$), in our case, $k_z \simeq \omega/(c\beta_{\mathrm{ph}})$ and the lack of confinement occur due to a lack of reflections (transverse impedance of adjacent layers is virtually identical).

This critical phenomenon could be advantageous depending on the application; transforming the transverse into longitudinal flow might be useful for coupling or combining laser beams for high-energy applications and, conversely, for sensors and spectrometry. In any case, the concept can be exploited to achieve controllable on-chip mode manipulations. Although this is not the focus of our study, it is reasonable to assume that a similar phenomenon may occur in metamaterials [32].

The concepts presented below apply to any quasi-periodic structure with a constant vacuum tunnel with applicable changes regarding the structure's specific parameters (geometry). The core conditions that must exist in order for the phenomenon to occur could be satisfied in any desired quasi-periodic geometry (circular or planar waveguide, photonic band gap, metamaterials, etc.). However, without significant loss of generality, throughout our analysis we adopt a geometry of a cylindrical Bragg waveguide in order to showcase the critical phenomenon's properties.

In a cylindrical Bragg reflection waveguide, the taper is facilitated by varying the thickness of all layers especially the first layer [33]. Adiabatic geometrical variations are tacitly assumed, and the local geometry of all layers determines the local phase velocity of the propagating wave (TM_{01} mode); azimuthally symmetric configuration is assumed.

A cylindrical Bragg reflection waveguide has a vacuum core radius of R_{int} and alternating layers of two dielectric coefficients of $\varepsilon_{\mathrm{I}}, \varepsilon_{\mathrm{II}}$. Although we tacitly assume pure, real, dielectric coefficients of existent materials, the concepts presented are also valid for artificial materials with effective coefficients, metamaterials, and photonic crystals.

By denoting the ν-th layer's dielectric coefficient as $\varepsilon_{r,\nu}$, the vacuum core ($\nu = 0$) has $\varepsilon_{r,0} = 1$ and the first dielectric layer ($\nu = 1$) has $\varepsilon_{r,1} = \varepsilon_{\mathrm{I}}$. Let "$z$" denote the waveguide's propagation axis and "r" the transverse coordinate. The longitudinal electric field of a TM_{01} mode with phase velocity β_{ph} is

$$E_{z,\nu} = \exp(-jk_z z) \times \begin{cases} E_0 J_0(k_{r,0} r) & \nu = 0 \\ A_\nu H_0^{(2)}(k_{r,\nu} r) + B_\nu H_0^{(1)}(k_{r,\nu} r) & \nu \ge 1 \end{cases}, \quad (1)$$

where the longitudinal wave-vector is $k_z = \omega/(c\beta_{\mathrm{ph}})$, and the transverse wave-vector is $k_{r,\nu} = \sqrt{\varepsilon_{r,\nu}(\omega/c)^2 - k_z^2}$.

In the vacuum core E_0 is the amplitude, and the amplitudes of the ν-th layer are A_ν, B_ν. J_0 is the Bessel function of the first kind, and $H_0^{(1)}$, $H_0^{(2)}$ are the Hankel functions of the first and second kind. The characteristic impedance of the vacuum core is $Z_0/\eta_0 = J_0(k_{r,0}R_{\mathrm{int}})/[J_c(k_{r,0}R_{\mathrm{int}})(\pi R_{\mathrm{int}}/\lambda)]$, where $\eta_0 = 377\,\Omega$, $J_c(x) = 2J_1(x)/x$ for $x > 0$, and 1 for $x = 0$. In a given layer ν, the transverse impedance is $Z_{\nu\ge1} = \eta_0\sqrt{\varepsilon_\nu - \beta_{\mathrm{ph}}^{-2}}/\varepsilon_\nu$.

For confinement, the width of each layer (and particularly the first layer) at a given phase velocity is derived from the following condition [33]:

Table 1. Parameters of the Envisaged Configuration

Parameter	Symbol	Value
Laser wavelength [μm]	λ	1
Internal radius [λ]	R_{int}	0.4
Dielectric constants	ε_{I}	3.9
	$\varepsilon_{\mathrm{II}}$	11.68
Cutoff velocity	$\beta^{(\mathrm{c.o.})}$	0.506
Critical velocity	β_{cr}	0.585
Number of layers	N	40

$$\begin{cases} E_{z,\nu}(r = R_\nu) = 0 & Z_\nu > Z_{\nu+1} \\ \partial_r E_{z,\nu}(r = R_\nu) = 0 & Z_\nu < Z_{\nu+1} \end{cases}. \quad (2)$$

Based on the boundary conditions, the dispersion relation $\mathcal{D}_N(\omega, k_z)$ is established [8], and it depends on an additional parameter: number of layers (subscript N). Figure 1(d) shows the result of such tapering—the thickness of *all* the layers decreases as the phase velocity β_{ph} increases. The configuration's parameters used for the numerical simulations are given in Table 1 (unless otherwise specified). Note that the first layer significantly varies if $\varepsilon_{r,1} = \varepsilon_{\mathrm{I}} < \varepsilon_{\mathrm{II}}$ and only slightly varies otherwise. In the latter case, the second layer would vary significantly.

In general, the allowed range of phase velocities spans from the cutoff (superscript c.o.) velocity $\beta^{(\mathrm{c.o.})} = \max(\beta_{\mathrm{I}}, \beta_{\mathrm{II}}) = 1/\sqrt{\min(\varepsilon_{\mathrm{I}}, \varepsilon_{\mathrm{II}})}$ to the speed of light, namely, $\beta_{\mathrm{ph}} \in [\beta^{(\mathrm{c.o.})}, 1]$. For instance, for an application of boosting particles from a sub-relativistic regime to the speed of light [29], a wide range of phase velocities would be required. In this case, the dielectric coefficients ($\varepsilon_{\mathrm{I}}, \varepsilon_{\mathrm{II}}$) should be as high as possible, such as zirconium dioxide (23) and silicon (11.68), which would permit a span of $\beta_{\mathrm{ph}} \in [0.293, 1]$.

In this span of phase velocities, special attention should be given to a *critical* phase velocity defined as

$$\beta_{\mathrm{cr}}^2 = \beta_{\mathrm{I}}^2 + \beta_{\mathrm{II}}^2 = \frac{1}{\varepsilon_{\mathrm{I}}} + \frac{1}{\varepsilon_{\mathrm{II}}}, \quad (3)$$

which occurs for $k_{r,\nu+1} \cdot \varepsilon_{r,\nu} = k_{r,\nu} \cdot \varepsilon_{r,\nu+1}$. Here, the characteristic impedances of adjacent layers are equal, $Z_\nu = Z_{\nu+1}$, whereas the transverse wave-vectors are different ($k_{r,\nu} \ne k_{r,\nu+1}$).

Figure 2 shows the characteristic impedances of layers made of zirconia (blue, $\varepsilon_{\mathrm{I}} = 3.9$) and silicon (green, $\varepsilon_{\mathrm{II}} = 11.68$) as a function of the phase velocity. Before the critical point β_{cr}, where the impedance of the first layer is smaller than the second layer ($Z_1 < Z_2$), the width of the first layer Δ_1 (red diamonds) decreases significantly as the velocity increases. Beyond β_{cr} ($Z_1 > Z_2$), Δ_1 slightly decreases as the velocity increases. Note that the layer's thickness in the vicinity of β_{cr} is discontinuous and the values converged from the left-hand side are different from the value converging from the right-hand side; we do not consider values in the close vicinity at β_{cr} since the taper can no longer be adiabatic. While our above analysis focused on the system's kinematics, next we investigate the system's dynamics by imposing boundary conditions for determining the field confinement. The electric field amplitudes A_ν, B_ν in any ν-th layer are calculated using the matrix method [8] for any given phase velocity. As shown in Fig. 3(a) for zirconia and silicon, the electric field's amplitude decays exponentially over 40 layers for $\beta_{\mathrm{ph}} \simeq 1$, whereas in Fig. 3(b) the amplitude virtually does not decay over 100 layers for $\beta_{\mathrm{ph}} = 0.58$ (close to the critical phase velocity $\beta_{\mathrm{cr}} = 0.585$). For the latter case,

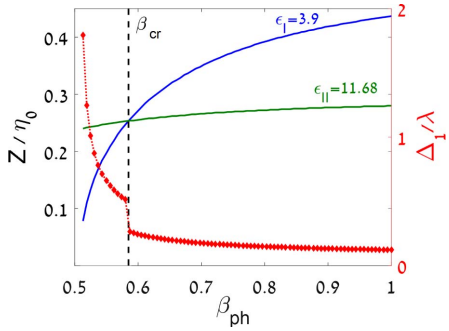

Fig. 2. Characteristic impedances of the first ($\varepsilon_{\mathrm{I}} = 3.9$) and second ($\varepsilon_{\mathrm{II}} = 11.68$) layers, and the corresponding width of the first layer (Δ_1) normalized to the wavelength (λ) in cylinder Bragg waveguide. At the critical point β_{cr}, where the impedances are equal, there is a discontinuity in the first layer's width.

neither of the conditions in Eq. (2) will lead to a transverse decay—thus, confinement can never be achieved.

In order to get an idea of the confinement dependence on the number of layers for any given phase velocity, the real part of the z-component electric field as a function of the former is shown in Fig. 4(a). Notably, around β_{cr} the mode is not confined in the radial direction—even in the case of 300 layers. Figure 4(b) shows the electromagnetic energy per unit length (W_{EM}) on the ν-th layer ($\nu = 10, 30, 50$) normalized to the maximum of ten layers as a function of the phase velocity. Increasing the number of layers results in orders of magnitude decay of the EM energy density at all phase velocities except the region adjacent to β_{cr} from both sides.

The formulation above tacitly assumes an infinite number of layers (N), thus, an ideal confinement. When N is finite, the confinement is no longer ideal as can be inferred from the dispersion relation $\mathcal{D}_N(\omega, k_z)$. The dispersion never zeros, but could be made arbitrarily small depending on the number of layers. Consequently, the longitudinal wavenumber k_z has an imaginary part, which grows as the phase velocity approaches β_{cr}; additional layers would reduce $\mathrm{Im}\{k_z\}$. Figure 5 shows the dispersion relation of the cylindrical Bragg structure for the parameters in Table 1. At $\beta_{\mathrm{ph}} = 1$ (blue curve), the imaginary part of k_z is negligible ($\mathrm{Im}\{k_z\} = 0.001 \times \omega/c$ for 40 layers), whereas close to the critical point (red curve) $\mathrm{Im}\{k_z\} = 0.195 \times \omega/c$ for the same number of layers. However, increasing the number of layers to 100 results in $\mathrm{Im}\{k_z\} = 0.001 \times \omega/c$. Evidently for a finite N, a longitudinally propagating power (P) is adiabatically transformed into transverse

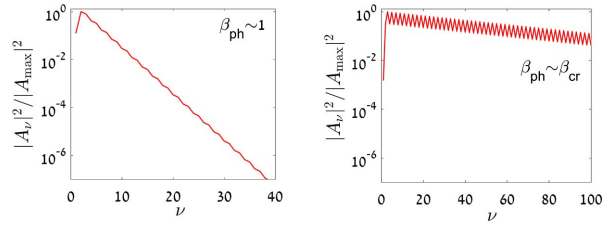

(a) Confinement **(b)** No confinement

Fig. 3. Electric field's amplitude versus the layer number: (a) amplitude decays exponentially over 40 layers for $\beta_{\mathrm{ph}} \simeq 1$ and (b) amplitude nearly does not decay over 100 layers for $\beta_{\mathrm{ph}} = 0.58$ ($\beta_{\mathrm{cr}} = 0.585$). Therefore, confinement is achieved only for the former case.

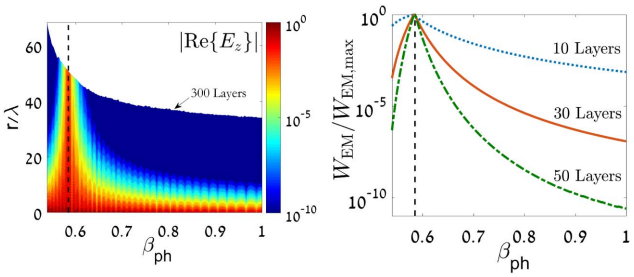

(a) Electric field **(b)** EM energy per unit length

Fig. 4. (a) Absolute value of the electric field's z-component (real part) propagating in a structure with 300 layers. (b) Electromagnetic energy per unit length (W_{EM}) on the ν-th layer ($\nu = 10, 30, 50$) normalized to the maximum EM energy per unit length for ten layers as a function of the phase velocity. Black dashed lines indicate β_{cr}, wherein confinement is not achieved.

propagation, which could be utilized as an electron-driven light source structure [34] or for transverse coupling.

In the following, we elaborate upon four topics: (i) field exponential decay, (ii) energy and group velocities, (iii) simulation with commercial electromagnetic code HFSS 18.0, and (iv) trade-offs associated with retaining the critical phase velocity outside of the required span of phase velocities.

First, for the case of β_{cr} being within a required range of phase velocities, we further investigate the field decay. As can be inferred from Fig. 3(a), the field decay r_c is exponential $\exp(-r/r_c)$. By denoting $L = [(\varepsilon_{\mathrm{I}} - \beta_{\mathrm{ph}}^{-2})^{-0.5} + (\varepsilon_{\mathrm{II}} - \beta_{\mathrm{ph}}^{-2})^{-0.5}]\lambda/4$ as the asymptotically ($N \to \infty$) periodic cell of two layers, the exponential decay r_c is $r_c/L = \left|\ln\left[\varepsilon_{\mathrm{I}}\sqrt{\varepsilon_{\mathrm{II}} - \beta_{\mathrm{ph}}^{-2}}/\left(\varepsilon_{\mathrm{II}}\sqrt{\varepsilon_{\mathrm{I}} - \beta_{\mathrm{ph}}^{-2}}\right)\right]\right|^{-1}$ [8]. Figure 6 shows r_c as a function of the phase velocity for the parameters in Table 1. It is evident that there is a weak decay (high r_c) in the region adjacent to β_{cr} from both sides [as shown in Fig. 4(b) as well]. Thus, the mode is adiabatically transformed from a guided mode to a non-confined mode.

Second, the energy ($v_{\mathrm{en}} = P/W_{\mathrm{EM}}$) and group velocities ($v_{\mathrm{gr}} = -(\partial\mathcal{D}/\partial k_z)/(\partial\mathcal{D}/\partial\omega)$) are equal in most cases except in phase velocity values in the vicinity of the critical point (not shown here due to space limitation). While the energy velocity

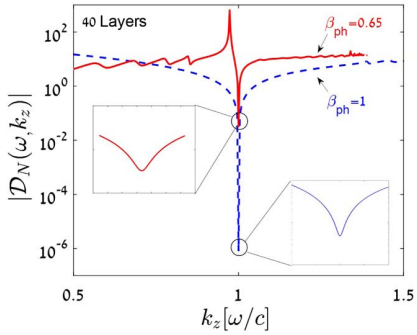

Fig. 5. Dispersion relation of cylindrical Bragg structure for the parameters in Table 1 as a function of the longitudinal wavenumber k_z for two phase velocities: speed of light (blue) and $\beta_{\mathrm{ph}} = 0.65$ (red). The imaginary part of k_z becomes more significant closer to the critical point ($\beta_{\mathrm{cr}} = 0.585$); adding more layers would reduce it minisculely.

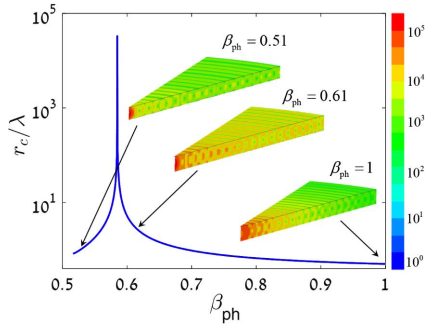

Fig. 6. Field decay r_c as a function of phase velocity for the parameters in Table 1. The insets are the output of HFSS simulation and the magnitude of the electric field for three phase velocities (0.51, 0.61, 1.0).

decreases as the phase velocity increases, the group velocity has an "infinite" derivative in the vicinity of the critical point.

Third, our analytical approach regarding the critical point phenomenon was verified with the commercial electromagnetic code HFSS 18.0. The cylindrical Bragg waveguide was modeled to obtain realistic field profiles of the propagating TM_{01} laser mode. For each phase velocity, the cylinder was simulated as an 18.0 slice with a symmetry condition to the slice's side planes to sort only the azimuthally symmetric modes. Master-slave boundary conditions were applied to simulate an infinite structure in the z-axis. The second mode was excited from the vacuum core toward the layers. Both the excited mode's frequency and the layers' width were set to match each phase velocity.

The insets in Fig. 6 plot the magnitude of the electric field in the Bragg structure for three values of phase velocity (0.51, 0.61, 1.0). Notably, far from the region adjacent to the critical point there is a transverse confinement. Around the critical point, the energy is less confined and radiation potentially could go into the vacuum surrounding the structure.

Last, for applications such as longitudinal coupling, particle acceleration, or light sources based on free electrons, it is required to preserve confinement for all β_{ph} values. This means that the critical phase velocity β_{cr} should be outside of the required range of phase velocities, i.e., $\beta_{cr} \le \beta^{(c.o.)} < 1$ or $\beta_{cr} > 1$. These conditions result in constraints on the combination of the dielectric materials. For example, the latter condition imposes $\varepsilon_{min} > 1$, $\varepsilon_{max} < (1 - \varepsilon_{min}^{-1})^{-1}$. However, by retaining $\beta_{cr} > 1$, the range of phase velocities narrows. On the other hand, to achieve a wide range of velocities, it is necessary to use materials with high dielectric coefficients, which would result in the critical point being within such range.

In conclusion, we demonstrated the existence of a critical behavior of a tapered quasi-periodic dielectric structure where a longitudinally propagating power is transformed into transverse propagation. It occurs around a critical phase velocity determined by the characteristic impedances of two adjacent layers, which should be equal. Regardless of the number of layers in the tapered structure, the mode is "leaking out," and its propagation constant is complex, similar to the case of a mode below cutoff. However, the difference between the two was clarified.

While the examples in this study focus on a dielectric Bragg reflection waveguide, similar behavior is anticipated in PBG structures as well as in metamaterials. Moreover, we discussed the unique behavior of the electromagnetic mode and its implications for several applications in integrated optics—sensors, spectrometry, coupling, and combining laser beams.

Funding. Israel Science Foundation (ISF); Rothschild Caesarea Foundation.

Acknowledgment. The authors thank Dr. Paul Pax for fruitful discussions regarding fabrication of tapered Bragg structures and Tomer Morgenstern and Omer Hamburger for preliminary discussions.

REFERENCES

1. A. C. Boucouvalas, IEEE J. Sel. Top. Quantum Electron. **22**, 0200203 (2016).
2. B. Redding and H. Cao, Opt. Lett. **37**, 3384 (2012).
3. C. Potts, T. W. Allen, A. Azar, A. Melnyk, C. R. Dennison, and R. G. DeCorby, Opt. Lett. **39**, 5941 (2014).
4. J. Brouckaert, W. Bogaerts, S. Selvaraja, P. Dumon, R. Baets, and D. Van Thourhout, IEEE Photon. Technol. Lett. **20**, 309 (2008).
5. R. J. England, R. J. Noble, B. Fahimian, B. Loo, E. Abel, A. Hanuka, and L. Schächter, AIP Conf. Proc. **1777**, 060002 (2016).
6. G. Mourou and T. Tajima, SPIE Newsroom (2012), pp. 10–11.
7. T. Tajima, W. Brocklesby, and G. Mourou, Opt. Photon. News **24**(5), 36 (2013).
8. A. Mizrahi and L. Schächter, Phys. Rev. E **70**, 016505 (2004).
9. E. C. Mägi, P. Steinvurzel, and B. J. Eggleton, Opt. Express **12**, 776 (2004).
10. J. C. Knight, T. A. Birks, P. St.J. Russell, and D. M. Atkin, Opt. Lett. **21**, 1547 (1996).
11. S. Huntington, J. Katsifolis, B. Gibson, J. Canning, K. Lyytikainen, J. Zagari, L. Cahill, and J. Love, Opt. Express **11**, 98 (2003).
12. G. Benoit, K. Kuriki, J.-F. Viens, J. D. Joannopoulos, and Y. Fink, Opt. Lett. **30**, 1620 (2005).
13. P. Yeh, A. Yariv, and E. Marom, J. Opt. Soc. Am. **68**, 1196 (1978).
14. K.-J. Kim, J.-K. Seo, and M.-C. Oh, Opt. Express **16**, 1423 (2008).
15. N.-S. Son, K.-J. Kim, J.-W. Kim, and M.-C. Oh, Opt. Express **20**, 827 (2012).
16. M. Skorobogatiy, K. Saitoh, and M. Koshiba, J. Opt. Soc. Am. B **21**, 2095 (2004).
17. A. Oskooi, A. Mutapcic, S. Noda, J. D. Joannopoulos, S. P. Boyd, and S. G. Johnson, Opt. Express **20**, 21558 (2012).
18. J. M. Castro, D. F. Geraghty, S. Honkanen, C. M. Greiner, D. Iazikov, and T. W. Mossberg, Opt. Express **13**, 4180 (2005).
19. P. Chiara and F. Frontera, Appl. Opt. **31**, 1361 (1992).
20. M. Kumar, T. Sakagichi, and F. Koyama, Appl. Phys. Lett. **94**, 061112 (2009).
21. B. Drobot, A. Melnyk, M. Zhang, T. Allen, and R. DeCorby, Opt. Express **20**, 23906 (2012).
22. A. Melnyk, Eureka **4**, 2 (2014).
23. L. Ma, T. Katagiri, and Y. Matsuura, Proc. SPIE **6351**, 63510Z (2006).
24. T. A. Birks and Y. W. Li, J. Lightwave Technol. **10**, 432 (1992).
25. R. P. Kenny, T. A. Birks, and K. P. Oakley, Electron. Lett. **27**, 1654 (1991).
26. E. Epp, N. Ponnampalam, W. Newman, B. Drobot, J. N. McMullin, A. F. Meldrum, and R. G. DeCorby, Opt. Express **18**, 24917 (2010).
27. R. G. DeCorby, N. Ponnampalam, E. Epp, T. Allen, and J. N. McMullin, Opt. Express **17**, 16632 (2009).
28. N. Ponnampalam and R. G. DeCorby, Opt. Express **16**, 2894 (2008).
29. A. Hanuka, C. Cohen, H. Lyabock, and L. Schächter, AIP Conf. Proc. **1812**, 100014 (2017).
30. A. W. Snyder and J. D. Love, *Optical Waveguide Theory* (Springer, 1983).
31. A. W. Snyder, D. J. Mitchell, A. Studies, and A. Mathematics, Optoelectronics **6**, 287 (1974).
32. N. Engheta and R. W. Ziolkowski, *Metamaterials: Physics and Engineering Explorations* (Wiley, 2006).
33. A. Mizrahi and L. Schächter, Opt. Express **12**, 3156 (2004).
34. V. Karagodsky, D. Schieber, and L. Schächter, Phys. Rev. Lett. **104**, 024801 (2010).